EUROPEAN ORGANIZATION FOR NUCLEAR RESEARCH

CERN-EP/86-195
24 November 1986

# DIRECT-PHOTON PLUS AWAY-SIDE JET PRODUCTION IN pp COLLISIONS AT $\sqrt{s}$ = 63 GeV AND A DETERMINATION OF THE GLUON DISTRIBUTION

*The Axial Field Spectrometer Collaboration*

T. Åkesson[5], M.G. Albrow[15], S. Almehed[9], E. Anassontzis[1], R. Batley[5], O. Benary[16], H. Bøggild[6], O. Botner[6], H. Breuker[5], V. Burkert[2], B. Callen[12], R. Carosi[5], A.A. Carter[14], J.R. Carter[4], P.C. Cecil[4], V. Chernyatin[10], Y. Choi[13], W.E. Cleland[13], S. Dagan[16], E. Dahl-Jensen[6], I. Dahl-Jensen[6], P. Dam[6], G. Damgaard[6], B. Dolgoshein[10], S. Eidelman[11], M.W. Evans[15], C.W. Fabjan[5], I. Gavrilenko[8], U. Goerlach[5], Y. Goloubkov[10], H. Gordon[3], K.H. Hansen[6], V. Hedberg[9], J.W. Hiddleston[15], P. Ioannou[1], G. Jarlskog[9], T. Jensen[5], A. Kalinovsky[10], V. Kantserov[10], S. Katsanevas[5], C. Kourkoumelis[1], R. Kroeger[13], K. Kulka[9], D. Lissauer[16], B. Lörstad[9], I. Mannelli[5], A. Markou[1], S. Mayburov[8], N.A. McCubbin[15], U. Mjörnmark[9], R. Møller[6], W. Molzon[12], P. Nevsky[10], B.S. Nielsen[5], L.H. Olsen[5], Y. Oren[16], G. Piskounov[11], D.C. Rahm[3], L.K. Resvanis [1], A. Rudge[5], J. Schukraft[5], A. Shmeleva[8], V. Sidorov[11], S. Smirnov[10], H. Specht[7], N. Starinsky[10], I. Stumer[3], M. Sullivan[13], H.H. Thodberg[6], J.A. Thompson[13], G. Thorstenson[9], A. Vanjashin[10], E. Vella[12], J. Williamson[15], W.J. Willis[5], M. Winik[3] and C. Woody[3]

(Submitted to Z. Phys. C)

1 University of Athens, Greece.
2 Physikalisches Institut, University of Bonn, Fed. Rep. Germany.
3 Brookhaven National Laboratory, Upton, NY, USA.
4 University of Cambridge, UK.
5 CERN, Geneva, Switzerland.
6 Niels Bohr Institute, University of Copenhagen, Denmark.
7 Physikalisches Institut, University of Heidelberg, Fed. Rep. Germany.
8 P.N. Lebedev Institute of Physics, Moscow, USSR.
9 University of Lund, Sweden.
10 Moscow Physical Engineering Institute, Moscow, USSR.
11 Institute of Nuclear Physics, Novosibirsk, USSR.
12 University of Pennsylvania, Philadelphia, Pa., USA.
13 University of Pittsburgh, Pa., USA.
14 Queen Mary College, London, UK.
15 Rutherford Appleton Laboratory, Didcot, UK.
16 University of Tel Aviv, Israel.

## ABSTRACT

We have determined the double inclusive cross-section for opposite-side high-$p_T$ photons and away-side jets with $\theta_\gamma \approx \theta_{jet} \approx 90°$ produced in pp collisions at the CERN Intersecting Storage Rings at $\sqrt{s} = 63$ GeV. Under the assumption that these events arise predominantly from the QCD gluon Compton process we have calculated the gluon structure function in the range $0.15 \leq x \leq 0.30$ at an average square of the four-momentum transfer of 40 $GeV^2/c^2$. The data favour a soft gluon distribution in the proton.

## 1. INTRODUCTION

Information on the momentum distribution of gluons inside nuclei [1, 2] and protons [3] has been obtained indirectly from deep inelastic lepton-scattering experiments. These experiments measure the quark and antiquark structure functions through the weak or electromagnetic interaction and make use of the scaling violation of quark structure functions to extract the gluon distribution. An independent and more direct way to measure the gluon structure function by using the strong interacting quarks as a probe has been proposed elsewhere [4–8]. Fritzsch and Minkowski emphasized the importance of the QCD Compton effects as a central test of QCD already in 1977. The main origin of high-$p_T$ direct photons, which were discovered in proton–proton collisions in 1979 [9, 10], is understood to be the QCD gluon Compton process ($qg \rightarrow \gamma q$). A measurement of the direct-photon spectrum alone does not allow one to extract the gluon distribution G(x). Such measurements at the Intersecting Storage Rings (ISR) [9–11] and the $p\bar{p}$ Collider [12] at CERN have however shown general agreement between the measured photon spectrum and that expected with input quark and gluon structure functions. An experiment at the Super Proton Synchrotron (SPS) [13] went further and, assuming a certain form $xG(x) = A(1 - x)^n$, fitted the data to find $n = 7 \pm 2$.

In the present experiment, by measuring both the photon and the recoil jet, we need make no assumption about the form of G(x). For $\theta_\gamma \approx \theta_{jet} \approx 90°$ the kinematics of the process $qg \rightarrow \gamma q$ is directly measured, with an event-by-event determination of $x_q \approx x_g$. In order to extract G(x), we still need to input the well-known quark-distribution function $F_2(x)$ and the theoretical QCD cross-section for the dominant process $qg \rightarrow \gamma q$.

The photons were detected in two high-granularity electromagnetic shower detectors (NaI) which were mounted inside a large hadron calorimeter. The recoil jet was measured by use of the calorimeter and drift chamber opposite to the photon detectors. Studies of the systematic errors in the present experiment have shown that the errors due to granularity limitations and energy-scale stability are larger than in the experiment R806 [11], which used liquid-argon calorimeters for the photon measurement. We have accordingly used the R806 inclusive photon cross-section and the photon–jet correlation presented in this paper to obtain the best determination of the gluon structure function.

## 2. APPARATUS

The experiment was performed with the Axial Field Spectrometer (AFS) [14, 15]. Figure 1 shows the arrangement of the detectors at the CERN ISR. The interaction region was surrounded by an inner hodoscope, consisting of 44 scintillation counters (not shown), a cylindrical drift chamber (DC), and a $2\pi$ uranium/copper/scintillator calorimeter (UCAL). For the detection of photons, the AFS was equipped with two high-granularity sodium iodide (NaI) walls covering a solid angle of twice 0.6 sr.

A magnetic field of 5 kG parallel to the direction of the colliding beams made a measurement of the momenta of charged particles possible. The drift chamber was azimuthally subdivided into 82 sectors of 4° containing 42 layers of sense wires. The DC angular acceptance was $2\pi$ (excluding two 16° wedges used for mechanical support) in azimuth and $\pm 1$ in rapidity. Track coordinates were measured in the transverse X–Y plane via drift time with a spatial resolution of 230 $\mu$m and via charge division in the Z (beam) direction giving a resolution of 1.5 cm. The achieved momentum resolution is $\Delta p/p \approx 0.025p$. During this analysis reconstructed tracks had to satisfy the criteria given in Table 1.

The calorimeter, consisting of a 6 radiation lengths electromagnetic part and a 3.6 absorption lengths hadronic part surrounded the drift chamber, matching its angular acceptance. A high granularity was achieved by the subdivision into towers of 20 cm × 20 cm. The readout was done via wavelength shifters on two sides of the towers for the electromagnetic and hadronic sections

separately. In test measurements an energy resolution of $\sigma(E)/E = 16\%/\sqrt{E}$ for electromagnetic and $37\%/\sqrt{E}$ for hadronic showers was obtained.

The photon detectors (NaI 1 and NaI 2; one opposite and one in the direction of the centre-of-mass motion) consisted of optically separated NaI crystals arranged in two walls of 20 × 30 elements at a distance of 107 cm from the interaction region [16]. The front faces of the crystals were 3.5 cm × 3.5 cm and their length (13.8 cm) corresponded to 5.3 radiation lengths. The total photon energy was measured by combining the three energy deposits in the NaI and the two uranium calorimeter sections behind.

The trigger system made use of the high granularity of the photon detectors by demanding (in coincidence with the event strobe defined by scintillators surrounding the beam pipe) a localized energy cluster above 1.9 GeV in the NaI and 1.3 GeV in the electromagnetic calorimeter part behind the NaI, respectively. As more than one cluster was allowed, high-$p_T$ $\pi^0$'s and $\eta$'s also triggered the system. The combined trigger threshold corresponds to approximately 4 GeV. The trigger was an OR between NaI 1 and NaI 2.

A description of the various on- and off-line calibration systems can be found elsewhere [15,16].

The data were obtained from proton–proton collisions at $\sqrt{s} = 63$ GeV during 28 ISR runs in 1983. The integrated luminosity was

$$\int L\,dt = 1.7 \times 10^{37}\,cm^{-2} \quad .$$

The recorded data consist of 1,008,544 events.

## 3. DATA ANALYSIS

### 3.1 Event selection

In the off-line analysis only events that passed a software energy threshold (Table 2) were processed through the standard AFS program chain. This includes pattern recognition in the NaI detectors and the uranium calorimeter, and tracking plus vertex reconstruction for charged particles in the drift chamber. Events were rejected if no vertex was found in the beam crossing region. The timing of the inner hodoscope and the beam–beam counters was required to be consistent with a single interaction, allowing no second interaction within ±30 ns of the nominal event time.

Additional filtering was done by demanding that an event must contain an isolated electromagnetic shower with no further shower above 180 MeV in the same NaI wall, or a good $\pi^0$ or $\eta$ candidate with the energies of the individual showers each being above 250 MeV.

The sample for data summary tape analysis contained 142,918 events. As the data were taken over the time period of one year we monitored the efficiency by the $\pi^0$ inclusive cross-section determined for all individual runs.

The full data analysis was done separately in all parts for each of the NaI detectors, and the results were found to be consistent within statistical errors. If not otherwise mentioned the combined results are presented here.

The selection criteria for single photons were as follows:

i) No track was allowed to point at the electromagnetic shower.

ii) No second shower above 180 MeV was tolerated in the same NaI wall unless it was a charged particle as indicated by a track.

iii) The shower radius was required to be within 8 to 25 mm.

iv) For the shower with the largest energy among all additional showers above 50 MeV, we checked that it did not combine with the single-photon candidate to form a $\pi^0$.

v) In order to decrease trigger-threshold effects a $p_T$ cut of 4.5 GeV/c was applied on the total reconstructed shower.

After this selection was applied, the total direct-photon candidate sample contained 13,590 events.

The $\pi^0$'s were identified with reasonable efficiencies up to our highest $p_T$ values as resolved pairs of photon showers. For the calculation of the $\gamma/\pi^0$ ratio the $\pi^0$'s had to satisfy the following requirements:

i) Both showers had to have an energy above 250 MeV.

ii) Showers with a track pointing towards them were not combined with others to form $\pi^0$ candidates.

iii) No third shower above 180 MeV was tolerated in the event unless it was a charged particle as indicated by a track.

iv) The two-photon mass had to be within $80 \leq m_{\gamma\gamma} \leq 190$ MeV.

v) $p_T > 4.5$ GeV/c.

The total selected $\pi^0$ statistics are 41,286 events.

Figure 2 shows the raw $\gamma/\pi^0$ ratio obtained. The indicated band shows the result of a Monte Carlo calculation which gives the remaining background from meson decays. There are three contributions to this background:

i) Meson decays where one shower fakes a direct-photon candidate as the second shower falls outside the detector.

ii) At high $p_T$ the two showers of a $\pi^0$ can be merged into one shower because of the finite resolution of the detector.

iii) Asymmetric decays where one shower has a small energy and thus escapes the analysis cuts.

The method to calculate this background has been described in detail elsewhere [17].

This event selection has been done in such a way that the result can be compared with previous measurements (experiment R806 [11]). For the present analysis the background to the QCD Compton process was further reduced by an 'anti-bremsstrahlung' or isolation selection: all events that had an additional electromagnetic shower above 180 MeV inside the NaI detector and outside, in a 40 cm wide veto region (corresponding to two uranium towers surrounding the NaI detector), were rejected. This cut was also applied if the additional shower was initiated by a charged particle as indicated by a DC track or if it was a clear hadronic shower with a fraction of electromagnetic energy above our limit. The motivations for this veto region cut were:

i) To reject events where the direct photon stems from a bremsstrahlung process and is accompanied by a hadronic jet. Owing to the geometry of our detector, jets were rejected in a cone around the photons with $\Delta\theta \approx \pm 35°$ and $\Delta\phi \approx \pm 40°$ (calculated for a photon in the centre of the NaI wall).

ii) To decrease further the background from $\pi^0$ and $\eta$ events where one shower falls outside the NaI detector.

After this final cut we found 7819 isolated single-photon candidates (background not subtracted). These were used to search for recoil jets as described in Section 3.2.

We have studied the effect of the veto region cut using Monte Carlo methods. The additional rejection of $\pi^0$ and $\eta$ decays was calculated assuming an ideal efficiency in the electromagnetic section of the uranium calorimeter.

The efficiency of rejecting bremsstrahlung events can only be estimated. Experimentally an upper limit of bremsstrahlung contribution was set by [18]: $\sigma$(bremsstrahlung $\gamma$)/$\sigma$(total $\gamma$) $< 0.3$ in the range $5.5 \leq p_T \leq 8.0$ GeV/c. A recent calculation [19] gives 23% as the sum over all bremsstrahlung contributions for pp scattering at $\sqrt{s} = 63$ GeV and a $p_T(\gamma)$ of 6 GeV/c.

The photon cross-section can now be calculated by subtracting the background and correcting for the total efficiency. The total $\gamma$ efficiency was calculated as the product of trigger probability, reconstruction efficiency, and geometrical acceptance (see Fig. 3). The result agrees with the inclusive photon cross-section from experiment R806 within 20%; however, when we study the systematic error, we find that the part of the background due to the merging of two photons from a $\pi^0$ is quite

sensitive to fine details in the simulation which are difficult to determine with sufficient precision. Because of this uncertainty in the background we choose to combine the R806 photon cross-section with the photon–jet correlation measured here.

### 3.2 Jet selection

The recoil jets to single-photon and $\pi^0$ triggers were identified by use of the UCAL information. The definition of a hadronic jet in our $p_T$ range is ambiguous. We made tests using different jet-finding algorithms, in particular for different threshold $p_T$(jet), and found for different algorithms the same corrected number of jets within $\pm 15\%$ that determines the systematic error. The final jet sample was obtained in the following way:

i) At least one charged particle with a $p_T > 200$ MeV/c was required in the hemisphere opposite to the trigger.

ii) All individual clusters with $\Delta\phi > 120°$ with respect to the trigger were summed up. The cut in $\Delta\phi$ was motivated by the energy flow (Fig. 4). Only clusters with a $p_T > 100$ MeV/c and a rapidity $|\eta| < 1$ were used. The jet momentum vector was formed as the vector sum of all clusters that satisfied these cuts.

iii) The transverse momentum of the jet was required to be $p_T(\text{jet}) > 4$ GeV/c. This requirement was chosen in order to decrease the dependence on the intrinsic parton $k_T$.

iv) All jets were restricted to the central region: $|\eta_{\text{jet}}| < 0.4$.

v) A negligible number of events were rejected by demanding $140° \leq \Delta\phi_{\gamma-\text{jet}} \leq 220°$.

After all these cuts we found 2307 direct-photon candidates with a central recoil jet. Event displays of typical photon–jet events are shown in Fig. 5. In Fig. 6 we show the $\Delta\phi$ distribution obtained from the photon direction and the jet axis.

No attempt was made to correct the jets for energy leakage and energy resolution of the calorimeter, or to subtract the underlying event structure, since these effects are not important in this analysis.

### 3.3 Photon–jet cross-section

The double inclusive photon–jet cross-section was calculated according to

$$(d^3\sigma/dp_T\, d\eta_\gamma\, d\eta_{\text{jet}})\big|_{\eta_\gamma=\eta_{\text{jet}}=0} = (d^2\sigma/dp_T\, d\eta_\gamma)\big|_{\eta_\gamma=0}\,(N_{\gamma-\text{jet}}/N_\gamma)/(\Delta\eta_{\text{jet}}\, R_{\text{jet}}) \quad ,$$

where $N_{\gamma-\text{jet}}/N_\gamma$ is the $\gamma$–jet correlation ratio and $R_{\text{jet}}$ the jet-detection correction factor, calculated for a rapidity bin of $|\eta_{\text{jet}}| \leq 0.4$ using the Lund Monte Carlo PYTHIA (see Section 4). The cross-section $(d^2\sigma/dp_T d\eta_\gamma)|_{\eta_\gamma=0}$ was taken from the experiment R806 [11]. The background contribution to the $\gamma$(candidate)–jet correlation ratio from $\pi^0$ and $\eta$ events was studied by a comparison of the $\gamma$(candidate)–jet and the $\pi^0$–jet correlation ratios. It has been shown [18, 20] that no difference is seen in the jets recoiling to a high-$p_T$ photon or $\pi^0$ in our $p_T$ range.

In our data sample we found no difference in the fragmentation functions of recoil jets for $\pi^0$ or photon events. In Fig. 7 we show the $\gamma$(candidate)–jet over the $\pi^0$–jet correlation which is consistent with being 1. Consequently, the $N_{\gamma(\text{candidate})-\text{jet}}/N_{\gamma(\text{candidate})}$ ratio shown in Fig. 8 coincides with the direct-$\gamma$–jet correlation (within a systematic error of $\pm 5\%$, taking the background as shown in Fig. 2 into account). The results for the direct-$\gamma$–away-side jet correlation and for the calculation of the photon away-side jet cross-section are given in Table 3. Systematic errors are given in Table 4. We estimate the total systematic error to be $\pm 28\%$.

A comparison of the photon–jet cross-section with a theoretical calculation is shown in Fig. 9. The calculation was done using the quark density of Ref. [3] and the gluon distribution of Ref. [1]. The $p_T$ dependence of our data is steeper compared to this lowest order QCD calculation.

We also calculated the cross-section (see Table 5)

$$d^3\sigma/d\eta_\gamma\, d\eta_{jet}\, dM \ ,$$

where M is the effective mass of the $\gamma$–jet system, and compared it with the two-jet cross-section [21] and the two-photon cross-section [22] measured under identical conditions with our apparatus (Fig. 10). The result is in qualitative agreement with the naïve expectation of differences of the order of the electromagnetic coupling constant.

## 4. MONTE CARLO SIMULATION

Two million events generated by the Lund Monte Carlo PYTHIA [23] were used in order to

i) calculate the jet-detection correction factor;
ii) estimate systematic dependences of our result (on the gluon distribution) on the accepted rapidity interval (deviations from 90° of $\theta_\gamma$ and $\theta_{jet}$);
iii) study the sensitivity on the intrinsic parton $k_T$;
iv) study the sensitivity to changes of the PYTHIA input gluon distribution.

PYTHIA simulates the hard scattering of free pointlike partons within colliding hadrons and produces final-state jets according to the Lund string model for fragmentation. For our purpose only events of the gluon Compton process or the annihilation process were generated. For the calculation of the jet-detection correction factor we used the Monte Carlo program with its standard parameters. These are structure functions taken from Gluck, Hoffmann and Reya [24], $Q^2 = (4/3)p_T^2$, $\Lambda_{QCD} = 0.3$, $\langle k_T \rangle = 0.44$ GeV/c, and a K factor of 1. The minimum transverse momentum on the parton level required for a parton to be scattered (QTMIN) was chosen to be 4 GeV. We checked that a lowering of this value to 3 GeV did not alter the result. The direct photon was required to fall into the NaI acceptance and the recoil jet into the above-defined rapidity bin of the jet acceptance. These events were passed through a simulation of the uranium calorimeter [15], taking into account realistic hadronic and electromagnetic shower profiles and a detailed description of the tower geometry including wavelength shifter readout and light sharing along a stack. Minimum-ionizing energy loss of charged particles, depth of interaction points, particle decays, electromagnetic and hadronic energy response and resolution, energy leakage out of the calorimeter, and the uranium noise were simulated.

After applying the same set of cuts as in the data analysis the correction factor was calculated as the ratio $N_{\gamma\text{–jet-found}}/N_{\gamma\text{–jet-generated}}$. The jet-detection correction factor as a function of the photon $p_T$ is shown in Fig. 11. We have determined the systematic error by investigating the magnitude of the loss of jets outside the acceptance in pseudorapidity, shown as a band in Fig. 11.

## 5. CALCULATION OF THE GLUON DISTRIBUTION

The photon–jet cross-section, where photon and recoil jet are detected close to $\theta = 90°$, is directly (without any normalization) proportional to the quark and gluon densities multiplied by the QCD interaction cross-section at the parton level [5]:

$$d\sigma/d\eta_\gamma\, d\eta_{jet}\, dp_T = (5\pi\alpha\alpha_s/3)\,[G(x,Q^2)F_2^{ep}(x,Q^2)/x^2s^{3/2}] \ ,$$

where

$$x = 2p_T/\sqrt{s} \ .$$

This formula neglects all non-gluon Compton contributions to the cross-section. We have shown in a previous publication [17], by a comparison of direct-photon production in pp and $p\bar{p}$ interactions,

that contributions from the annihilation process are small (below $p_T$ values of 6 GeV/c). A recent calculation [19] attributes a contribution of 8.7% of the annihilation process to the total photon cross-section. Contributions from bremsstrahlung processes were suppressed in this analysis, as described in Section 3.1.

As the input for our calculation we used the quark density as measured with high precision by the European Muon Collaboration [3], using hydrogen targets.

The choice of the variable $Q^2$ is ambiguous in hadronic interactions. We used three different scales, $Q^2 = p_T^2$, $Q^2 = (4/3)p_T^2$, and $Q^2 = 2p_T^2$ in order to estimate the dependence of our result ($\pm 8\%$). The final calculation was done with $Q^2 = (4/3)p_T^2$.

The QCD scale parameter $\Lambda$ and the gluon distribution are strongly correlated and cannot be determined independently. We varied $\Lambda$ in the range 0.1 to 0.4 GeV, finding a variation of $\pm 15\%$ on our result. Our final choice was $\Lambda = 0.2$ GeV.

Several different approaches were made in order to describe the R806 inclusive photon cross-section [11] by QCD. Aurenche et al. [25] made a QCD calculation beyond the leading logarithmic approximation including all second-order diagrams. Contogouris et al. [26] derive rules to determine K factors (first introduced to describe the discrepancy between the QCD prediction of lepton-pair production via the Drell–Yan process and the experimental data) for all large transverse-momentum processes. Both methods lead to a satisfactory agreement with the data, however giving somewhat too low predictions at low $p_T$.

In this analysis we account for the higher order corrections by a K factor of 2.

### 5.1 Result and discussion

We have calculated xG with $\alpha_s = 12\pi/[25 \ln (Q^2/\Lambda^2)]$ where $Q^2 = (4/3)\, p_T^2$ and $\Lambda = 0.2$ GeV. Our result of xG is given in Table 6 for the individual $(x,Q^2)$ bins and compared with the CDHS result [1] in Fig. 12, where we also show statistic and systematic errors. The systematic errors are the quadratic combination of the errors on the photon–jet cross-section and the uncertainty due to the choice of the scale $Q^2$ and the $\Lambda$ parameter.

For the comparison the gluon distribution of CDHS was calculated for our $(x, Q^2)$ bins. Comparing the slope of the CDHS gluon distribution with our data points we find an indication for a softer distribution from our data. We note that a lower value of the hard-gluon abundance is also consistent with a measurement of the gluon/quark ratio in dijet production [21], using charge correlations in the jet fragmentation to identify quarks and gluons.

An extraction of the $Q^2$ dependence from our data is not feasible because all data were obtained at the same centre-of-mass energy (63 GeV) and scattering angle.

## 6. CONCLUSIONS

We have measured the invariant cross-section for opposite-side high-$p_T$ photons and away-side jets around $\theta_\gamma \approx \theta_{jet} \approx 90°$. We have shown that under the assumption that these events arise from the QCD gluon Compton process a direct determination of the gluon structure function is feasible. Our result indicates a softer gluon distribution when compared to the structure function extrapolated from deep inelastic neutrino scattering (CDHS) in the range $0.15 \leq x \leq 0.3$.

**Acknowledgements**

We wish to thank the ISR Experimental Support and Operations Groups for providing excellent conditions throughout this experiment. We thank G. Ingelman for his help with the Lund Monte Carlo programs, and R. Baier, A.P. Contogouris and A. Zhilin for stimulating discussions. Support from the Research Councils in our home countries is gratefully acknowledged.

## REFERENCES


[1] H. Abramowicz et al., Z. Phys. **C12**, 289 (1982).
P. Buchholz, private communication, 1985.
[2] F. Bergsma et al., Phys. Lett. **123B**, 269 (1983).
F. Bergsma et al., Phys. Lett. **153B**, 111 (1985).
[3] J.J. Aubert et al., Nucl. Phys. **B259**, 189 (1985).
[4] H. Fritzsch and P. Minkowski, Phys. Lett. **69B** 316 (1977).
[5] F. Halzen, M. Dechantsreiter and D.M. Scott, Phys. Rev. **D22**, 1617 (1980).
[6] L. Cormell and J.F. Owens, Phys. Rev. **D22**, 1609 (1980).
[7] R. Baier, J. Engels and B. Petersson, Z. Phys. **C6**, 309 (1980).
P. Aurenche et al., Phys. Lett. **169B**, 441 (1986).
[8] A.V. Vanyashin, A.V. Zhilin and Yu.P. Nikitin, Sov. J. Nucl. Phys. **39**, 608 (1984).
[9] M. Diakonou et al., Phys. Lett. **87B**, 292 (1979).
M. Diakonou et al., Phys. Lett. **91B**, 296 (1980).
[10] A.L.S. Angelis et al., Phys. Lett. **94B**, 106 (1980).
[11] E. Anassontzis et al., Z. Phys. **C13**, 277 (1982).
[12] J.A. Appel et al., Phys. Lett. **B176**, 239 (1986).
[13] J. Badier et al., Z. Phys. **C31**, 341 (1986).
[14] H. Gordon et al., Nucl. Instrum. Methods **196**, 303 (1982).
O. Botner et al., Nucl. Instrum. Methods **196**, 314 (1982).
O. Botner et al., Nucl. Instrum. Methods **179**, 45 (1981).
[15] T. Åkesson et al., Nucl. Instrum. Methods **A241**, 17 (1985).
[16] R. Batley et al., Nucl. Instrum. Methods **A242**, 75 (1985).
[17] T. Åkesson et al., Phys. Lett. **158B**, 282 (1985).
[18] T. Åkesson et al., Phys. Lett. **118B**, 178 (1982).
[19] E.L. Berger, E. Braaten and R.D. Field, Nucl. Phys. **B239**, 52 (1984).
[20] T. Åkesson et al., Phys. Scr. **34**, 106 (1986).
[21] T. Åkesson et al., Z. Phys. **C30**, 27 (1986).
[22] T. Åkesson et al., preprint CERN-EP/86-37, submitted to Z. Phys. C.
[23] H.U. Bengtsson and G. Ingelman, Computer Phys. Commun. **34**, 251 (1985).
[24] M. Gluck, E. Hoffmann and E. Reya, Z. Phys. **C13**, 119 (1982).
[25] P. Aurenche et al., Phys. Lett. **140B**, 87 (1984).
[26] A.P. Contogouris and H. Tanaka, Phys. Rev. **D33**, 1265 (1986).
A.P. Contogouris, S. Papadopoulos and J. Ralston, Phys. Lett. **104B**, 70 (1981).
A.P. Contogouris, S. Papadopoulos and J. Ralston, Phys. Rev. **D25**, 1280 (1982).

**Table 1**

Drift-chamber track-quality cuts

| | |
|---|---|
| 1) | Length of track $> 25$ cm |
| 2) | First digitizing within 32 cm from the interaction region |
| 3) | $\chi^2$/number of degrees of freedom $< 10$ |
| 4) | Track to point at the common event vertex |
| 5) | Rapidity of track $\lvert\eta\rvert \leqslant 0.9$. |

**Table 2**

Software energy thresholds (GeV)

| | NaI 1 | NaI 2 |
|---|---|---|
| $E_{tot}$ [a)] | 3.1 | 3.9 |
| $E_{NaI}$ | 1.7 | 2.0 |
| $E_{UCALem}$ | 1.0 | 1.4 |

a) Energy summed up as NaI + $UCAL_{em}$ + $UCAL_{had}$.

**Table 3**

Direct photon–jet cross-section

| $p_T$ (GeV/c) | $\gamma$–jet correlation $(N_{\gamma-jet}/N_\gamma)\,(1/R_{jet})$ | $d\sigma/d\eta_\gamma d\eta_{jet} dp_T)$ $(cm^2/GeV)$ | Statistical error |
|---|---|---|---|
| 4.71 | $0.269 \pm 0.009$ | $4.66 \times 10^{-33}$ | $\pm 1.56 \times 10^{-34}$ |
| 5.21 | $0.288 \pm 0.010$ | $2.42 \times 10^{-33}$ | $\pm 8.42 \times 10^{-35}$ |
| 5.71 | $0.325 \pm 0.014$ | $1.38 \times 10^{-33}$ | $\pm 5.99 \times 10^{-35}$ |
| 6.21 | $0.346 \pm 0.018$ | $7.79 \times 10^{-34}$ | $\pm 4.20 \times 10^{-35}$ |
| 6.71 | $0.375 \pm 0.022$ | $4.60 \times 10^{-34}$ | $\pm 2.70 \times 10^{-35}$ |
| 7.21 | $0.322 \pm 0.027$ | $2.20 \times 10^{-34}$ | $\pm 1.78 \times 10^{-35}$ |
| 7.71 | $0.398 \pm 0.036$ | $1.58 \times 10^{-34}$ | $\pm 1.40 \times 10^{-35}$ |
| 8.21 | $0.338 \pm 0.051$ | $7.87 \times 10^{-35}$ | $\pm 1.21 \times 10^{-35}$ |
| 8.71 | $0.395 \pm 0.064$ | $5.38 \times 10^{-35}$ | $\pm 8.97 \times 10^{-36}$ |
| 9.74 | $0.546 \pm 0.031$ | $2.94 \times 10^{-35}$ | $\pm 4.06 \times 10^{-36}$ |

**Table 4**

Systematic errors on $d\sigma/d\eta_\gamma d\eta_{jet} dp_T$ (%)

| | | |
|---|---|---|
| 1) | The inclusive photon cross-section from Ref. [11] | 20 |
| 2) | The jet-finding correction-factor calculation | 10 |
| 3) | The different algorithms of the jet selection | 15 |
| 4) | The background substraction in $N_{\gamma-jet}/N_\gamma$ | 5 |
| 5) | The absolute energy-scale uncertainty | 5 |

**Table 5**

Photon–jet mass cross-section

| M ($GeV/c^2$) | $d\sigma/d\eta_\gamma d\eta_{jet} dM$ ($cm^2/GeV$) | Statistical error | Systematic error |
|---|---|---|---|
| 10.7 | $1.34 \times 10^{-33}$ | $\pm 8.71 \times 10^{-35}$ | $\pm 4.26 \times 10^{-34}$ |
| 11.2 | $1.12 \times 10^{-33}$ | $\pm 7.84 \times 10^{-35}$ | $\pm 3.56 \times 10^{-34}$ |
| 11.7 | $1.07 \times 10^{-33}$ | $\pm 7.49 \times 10^{-35}$ | $\pm 3.03 \times 10^{-34}$ |
| 12.2 | $7.90 \times 10^{-34}$ | $\pm 6.32 \times 10^{-35}$ | $\pm 2.24 \times 10^{-34}$ |
| 12.7 | $6.07 \times 10^{-34}$ | $\pm 4.92 \times 10^{-35}$ | $\pm 1.72 \times 10^{-34}$ |
| 13.2 | $5.02 \times 10^{-34}$ | $\pm 4.97 \times 10^{-35}$ | $\pm 1.42 \times 10^{-34}$ |
| 13.7 | $4.55 \times 10^{-34}$ | $\pm 4.60 \times 10^{-35}$ | $\pm 1.29 \times 10^{-34}$ |
| 14.2 | $3.04 \times 10^{-34}$ | $\pm 3.68 \times 10^{-35}$ | $\pm 8.60 \times 10^{-35}$ |
| 14.7 | $2.75 \times 10^{-34}$ | $\pm 3.52 \times 10^{-35}$ | $\pm 7.78 \times 10^{-35}$ |
| 15.2 | $1.50 \times 10^{-34}$ | $\pm 2.54 \times 10^{-35}$ | $\pm 4.25 \times 10^{-35}$ |
| 15.7 | $1.25 \times 10^{-34}$ | $\pm 2.50 \times 10^{-35}$ | $\pm 3.54 \times 10^{-35}$ |
| 16.3 | $9.40 \times 10^{-35}$ | $\pm 1.50 \times 10^{-35}$ | $\pm 2.66 \times 10^{-35}$ |
| 17.3 | $4.61 \times 10^{-35}$ | $\pm 1.03 \times 10^{-35}$ | $\pm 1.30 \times 10^{-35}$ |
| 18.3 | $4.46 \times 10^{-35}$ | $\pm 1.12 \times 10^{-35}$ | $\pm 1.26 \times 10^{-35}$ |
| 19.3 | $2.73 \times 10^{-35}$ | $\pm 8.63 \times 10^{-36}$ | $\pm 7.73 \times 10^{-36}$ |

**Table 6**

Calculation of xG data points (K = 2)

| x | $Q^2$ | $\alpha_s$ | $F_2$ | xG | Systematic error on xG |
|---|---|---|---|---|---|
| 0.15 | 29.58 | 0.228 | 0.331 | 1.73 | ± 0.51 |
| 0.17 | 36.19 | 0.222 | 0.327 | 1.27 | ± 0.37 |
| 0.18 | 43.47 | 0.216 | 0.321 | 1.00 | ± 0.30 |
| 0.20 | 51.42 | 0.211 | 0.314 | 0.76 | ± 0.23 |
| 0.21 | 60.03 | 0.206 | 0.307 | 0.59 | ± 0.17 |
| 0.23 | 69.31 | 0.202 | 0.298 | 0.37 | ± 0.11 |
| 0.25 | 79.26 | 0.199 | 0.288 | 0.34 | ± 0.10 |
| 0.26 | 89.87 | 0.195 | 0.278 | 0.22 | ± 0.07 |
| 0.28 | 101.15 | 0.193 | 0.269 | 0.18 | ± 0.05 |
| 0.31 | 126.49 | 0.187 | 0.246 | 0.16 | ± 0.04 |

**Figure captions**

**Fig. 1** Experimental set-up.

**Fig. 2** Uncorrected $\gamma/\pi^0$ ratio and result of the background calculation. The dashed line indicates the actually subtracted background.

**Fig. 3** Total photon efficiency.

**Fig. 4** Example for the energy flow measured in the UCAL in direct-photon events.

**Fig. 5** Typical photon–jet events: a) momentum vectors in the X–Y plane; b) momentum vectors in the X–Z plane; c) after track fitting in the central DC (solid lines DC, dashed lines UCAL, dotted lines NaI). The photon is presented by two momentum vectors: dotted for the fraction of its energy detected in the NaI, and dashed for the fraction of its energy seen in the electromagnetic part of the UCAL. Note the different scale.

**Fig. 6** $\Delta\phi$ photon–jet axis (r.m.s. = 11.5° and mean = 180.0°).

**Fig. 7** $\gamma$–jet over $\pi^0$–jet correlation.

**Fig. 8** $\gamma$–jet correlation.

**Fig. 9** Double inclusive photon–jet cross-section and comparison with lowest order QCD prediction.

**Fig. 10** Comparison of photon–jet mass cross-section with two-jet and two-photon cross-sections.

**Fig. 11** Jet-detection correction factor as a function of the photon $p_T$. The systematic uncertainty is indicated by the two outer lines.

**Fig. 12** Result on the gluon distribution and comparison with CDHS [1]. The systematic errors are indicated by $\sqsupset$.

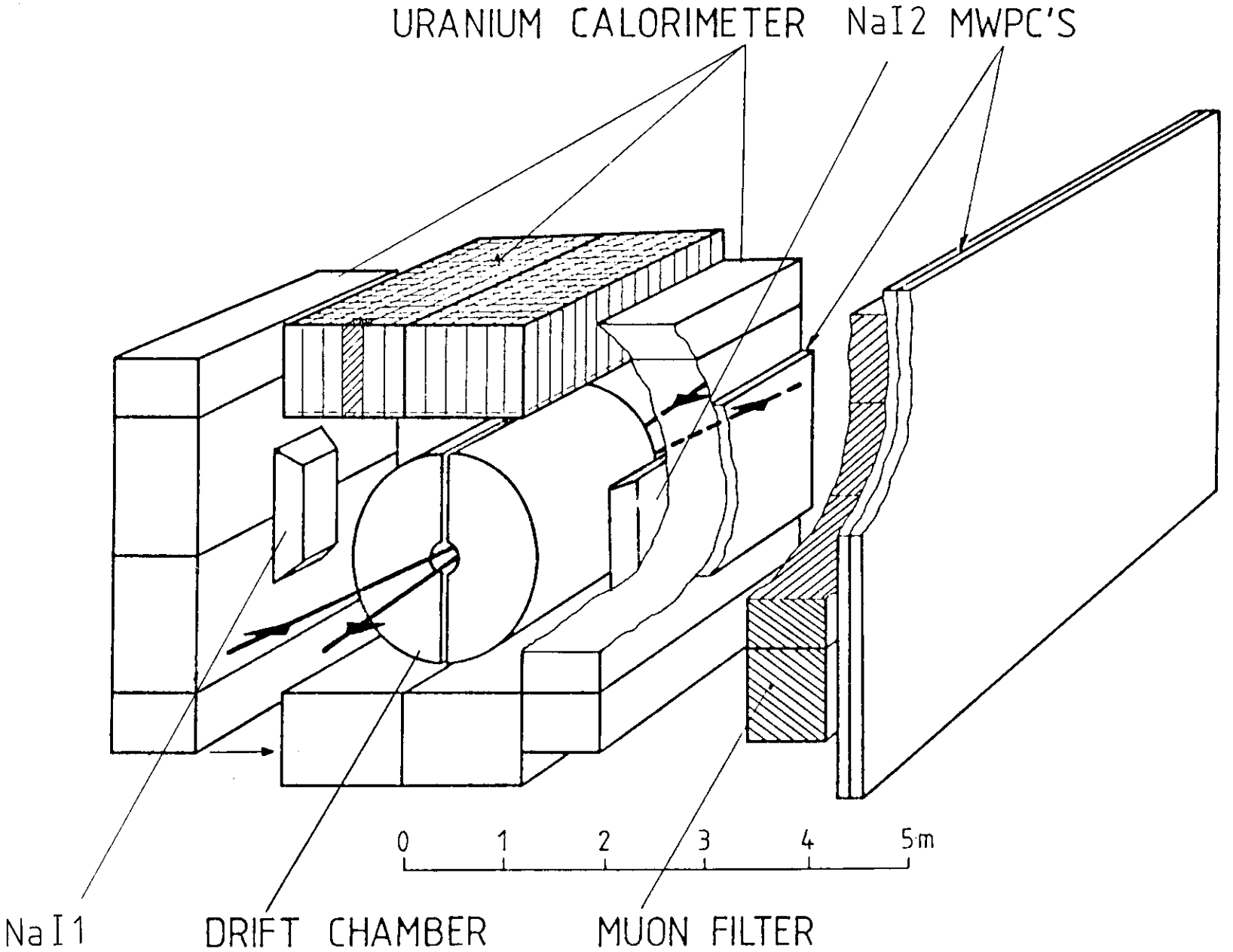
URANIUM CALORIMETER
NaI2 MWPC'S
0
1
2
3
4
5m
NaI1
DRIFT CHAMBER
MUON FILTER

**Fig. 1**

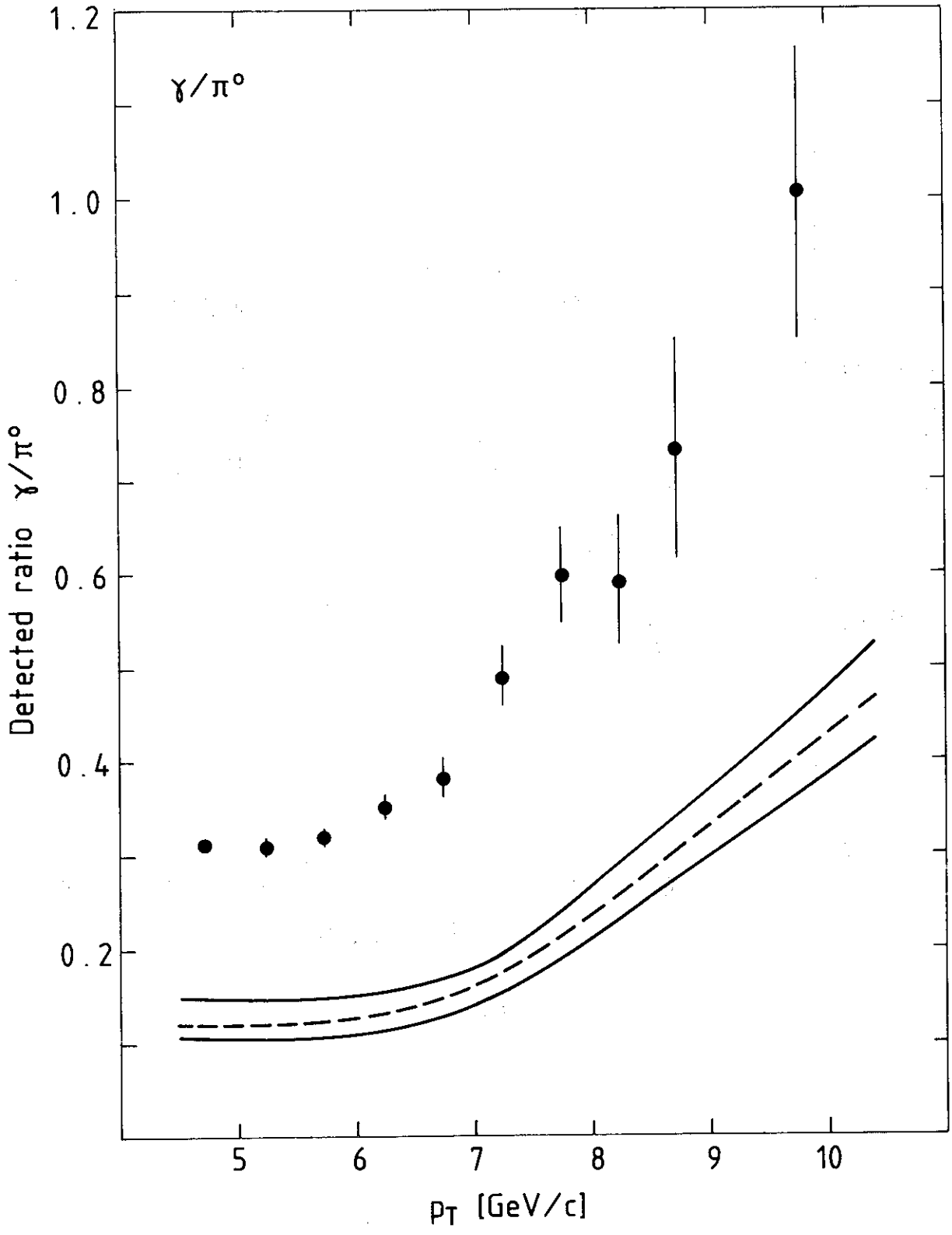


**Fig. 2**

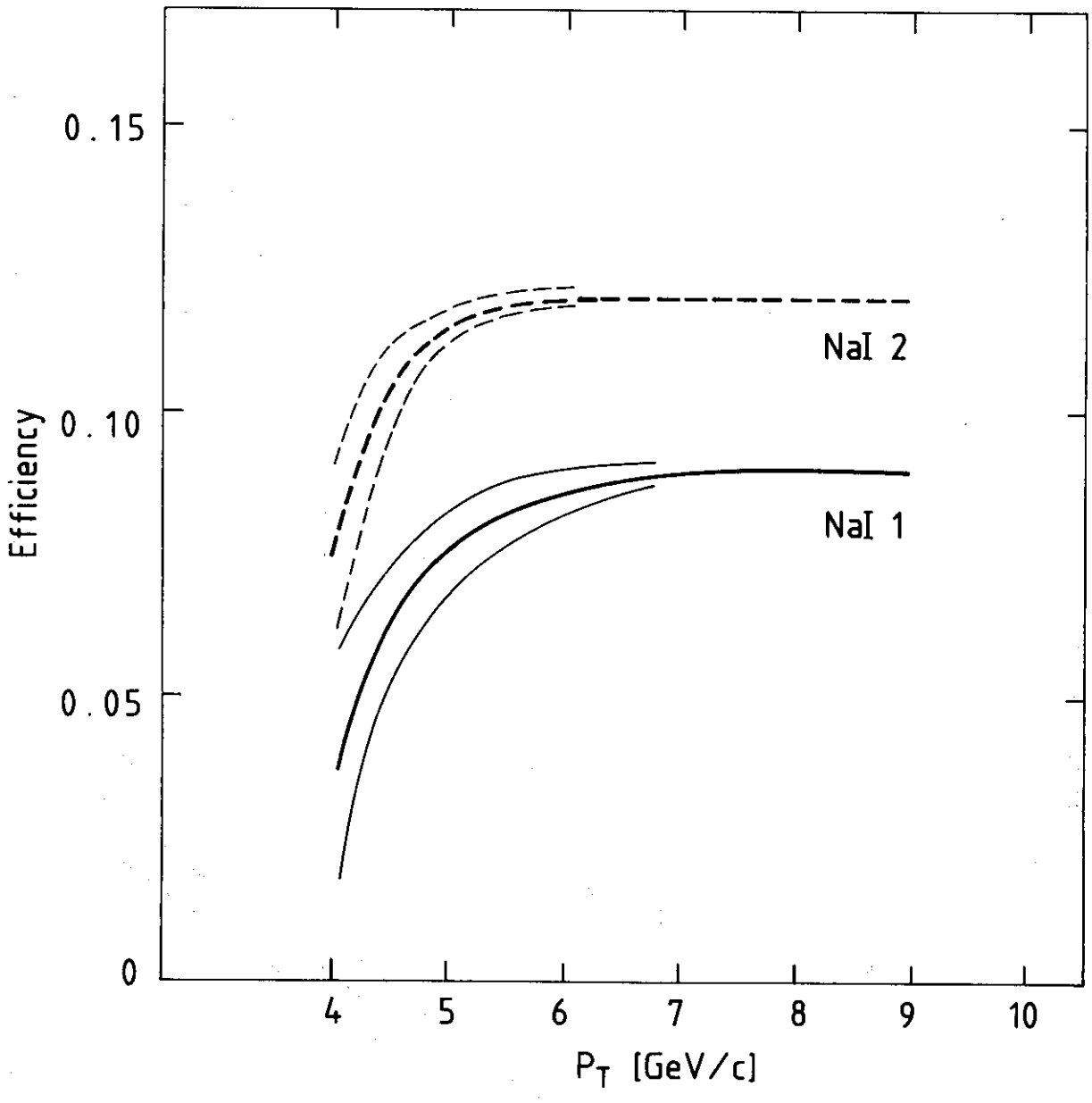


**Fig. 3**

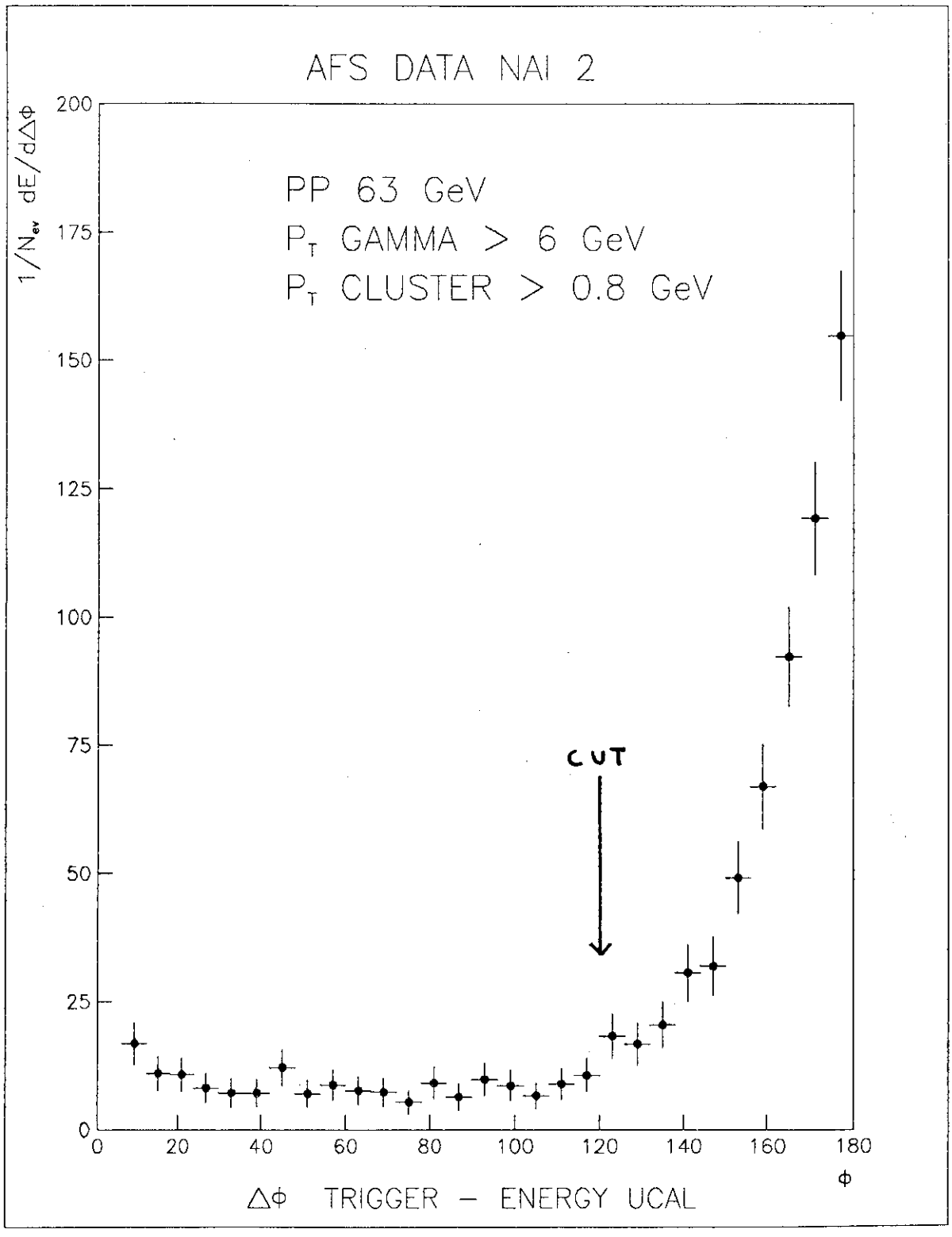
AFS DATA NAI 2
PP 63 GeV
$P_T$ GAMMA > 6 GeV
$P_T$ CLUSTER > 0.8 GeV
CUT
$1/N_{ev}\ dE/d\Delta\phi$
200
175
150
125
100
75
50
25
0
0
20
40
60
80
100
120
140
160
180
$\phi$
$\Delta\phi$ TRIGGER – ENERGY UCAL

**Fig. 4**

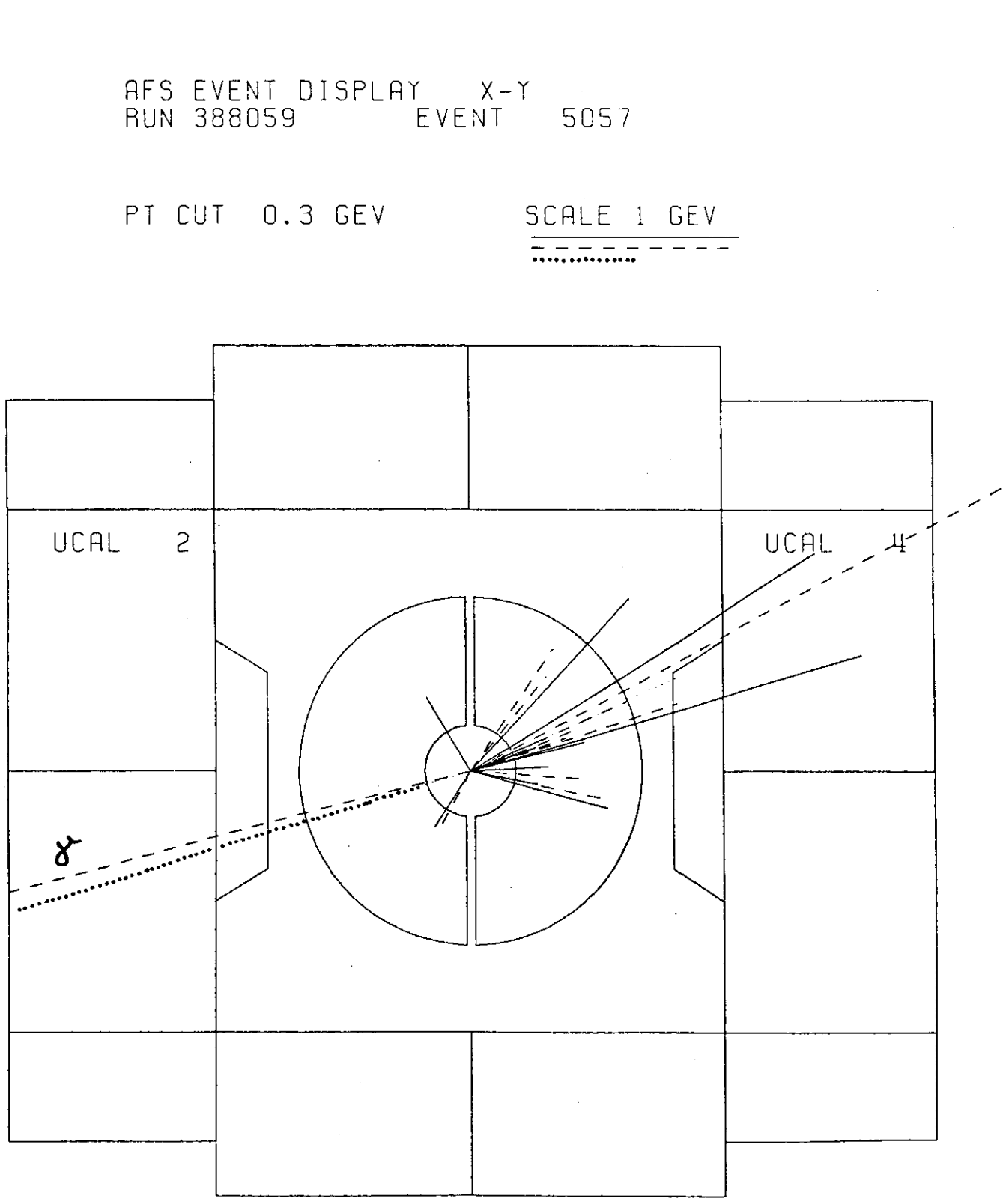
AFS EVENT DISPLAY X-Y
RUN 388059 EVENT 5057
PT CUT 0.3 GEV
SCALE 1 GEV
UCAL 2
UCAL 4
γ

**Fig. 5 a)**

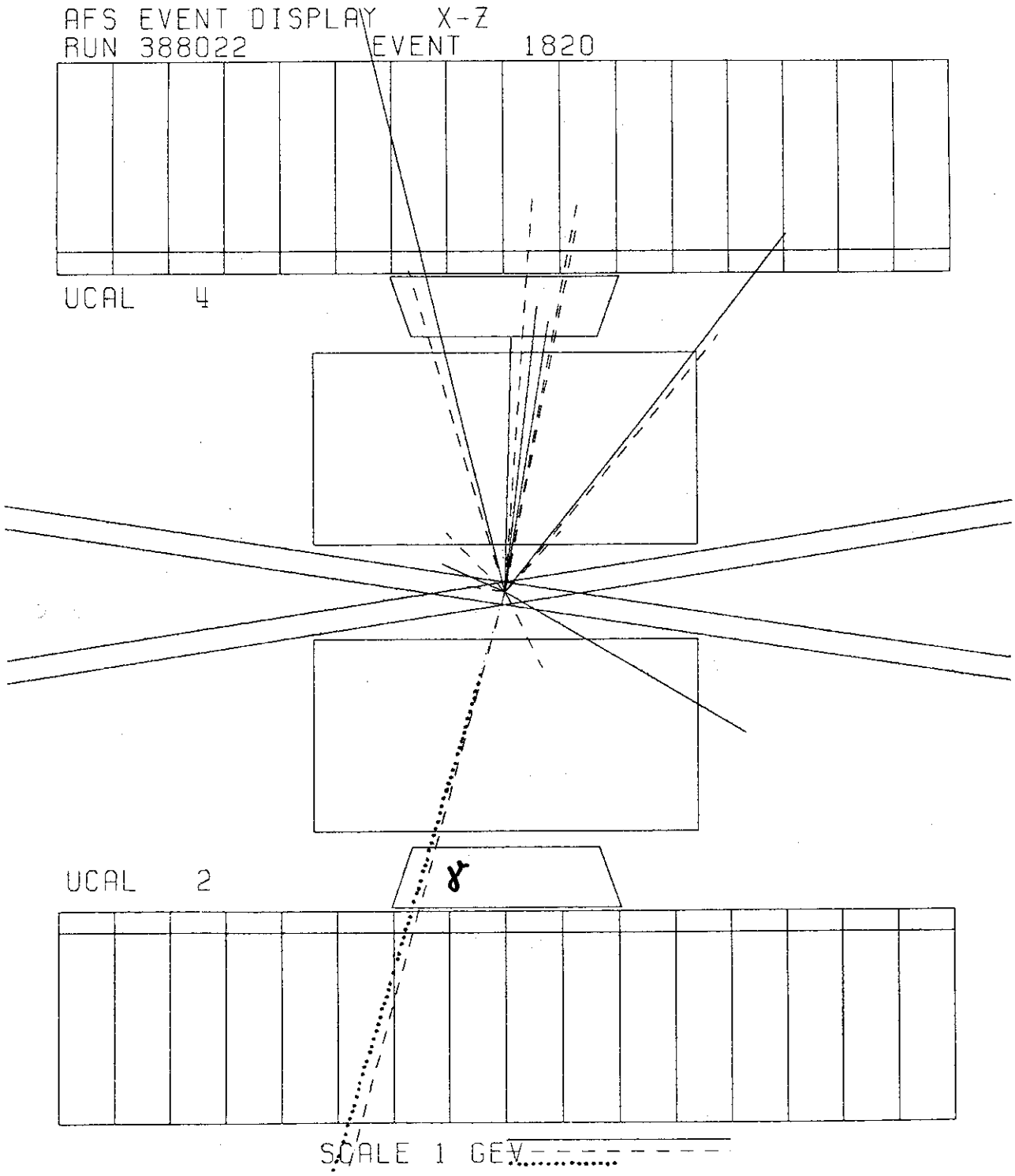
AFS EVENT DISPLAY X-Z
RUN 388022 EVENT 1820
UCAL 4
UCAL 2
γ
SCALE 1 GEV

**Fig. 5** b)

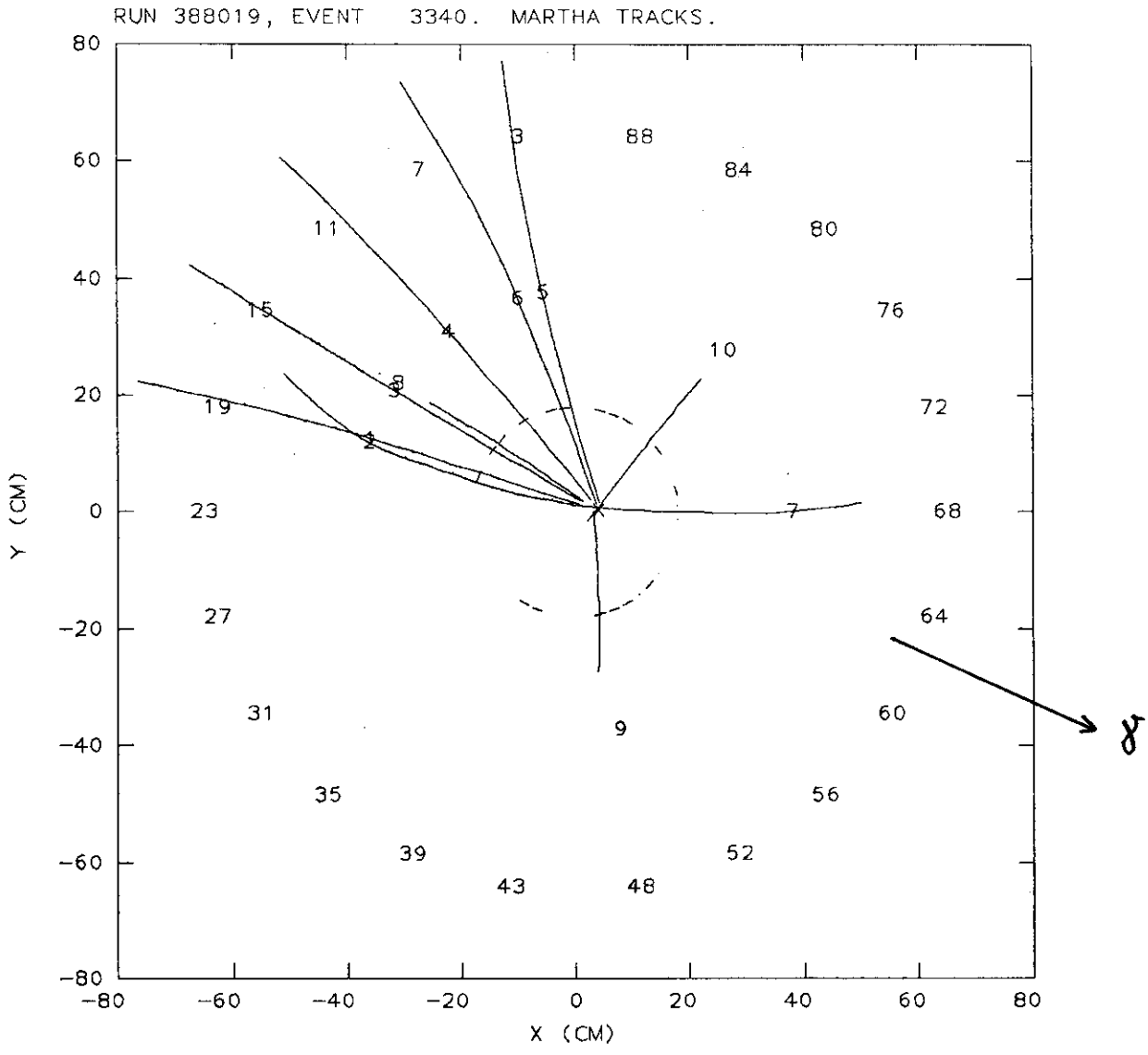
RUN 388019, EVENT 3340. MARTHA TRACKS.
Y (CM)
X (CM)
80
60
40
20
0
-20
-40
-60
-80
-80
-60
-40
-20
0
20
40
60
80
88
84
80
76
72
68
64
60
56
52
48
43
39
35
31
27
23
19
15
11
7
3
10
9
γ

**Fig. 5 c)**

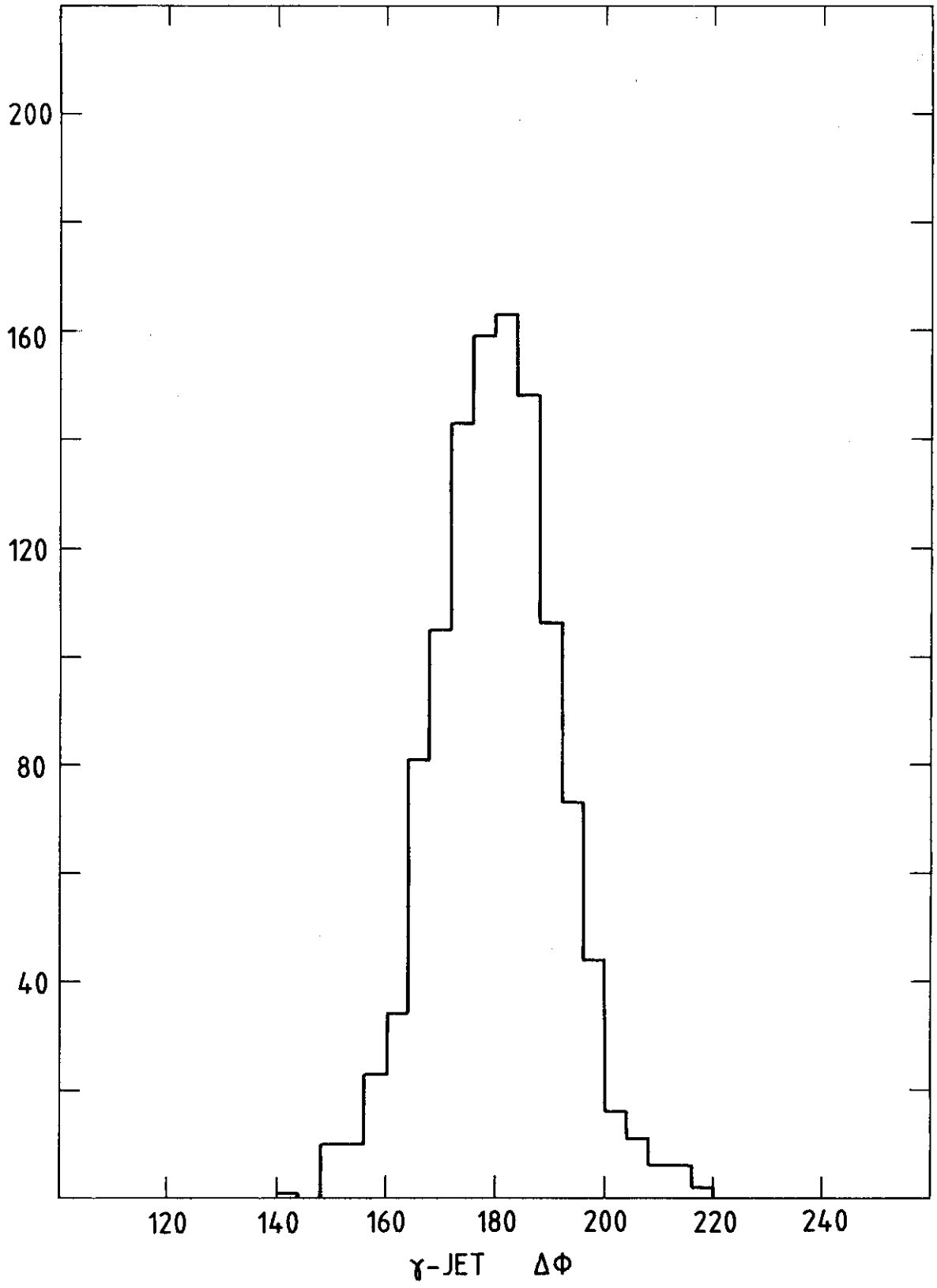


Fig. 6

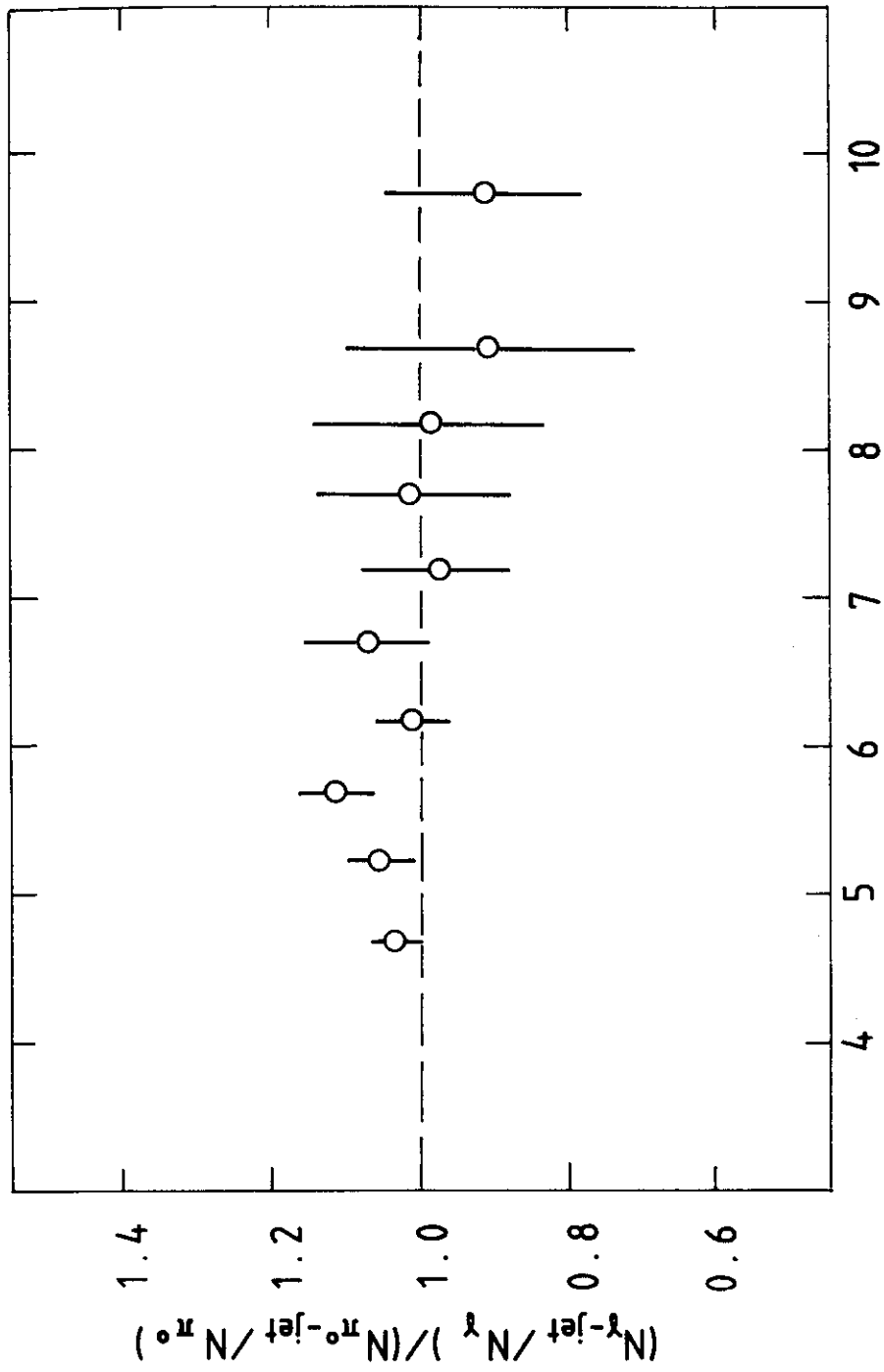
$(N_{\gamma\text{-jet}}/N_{\gamma})/(N_{\pi^0\text{-jet}}/N_{\pi^0})$
1.4
1.2
1.0
0.8
0.6
4
5
6
7
8
9
10
$p_T$ [GeV/c]

Fig. 7

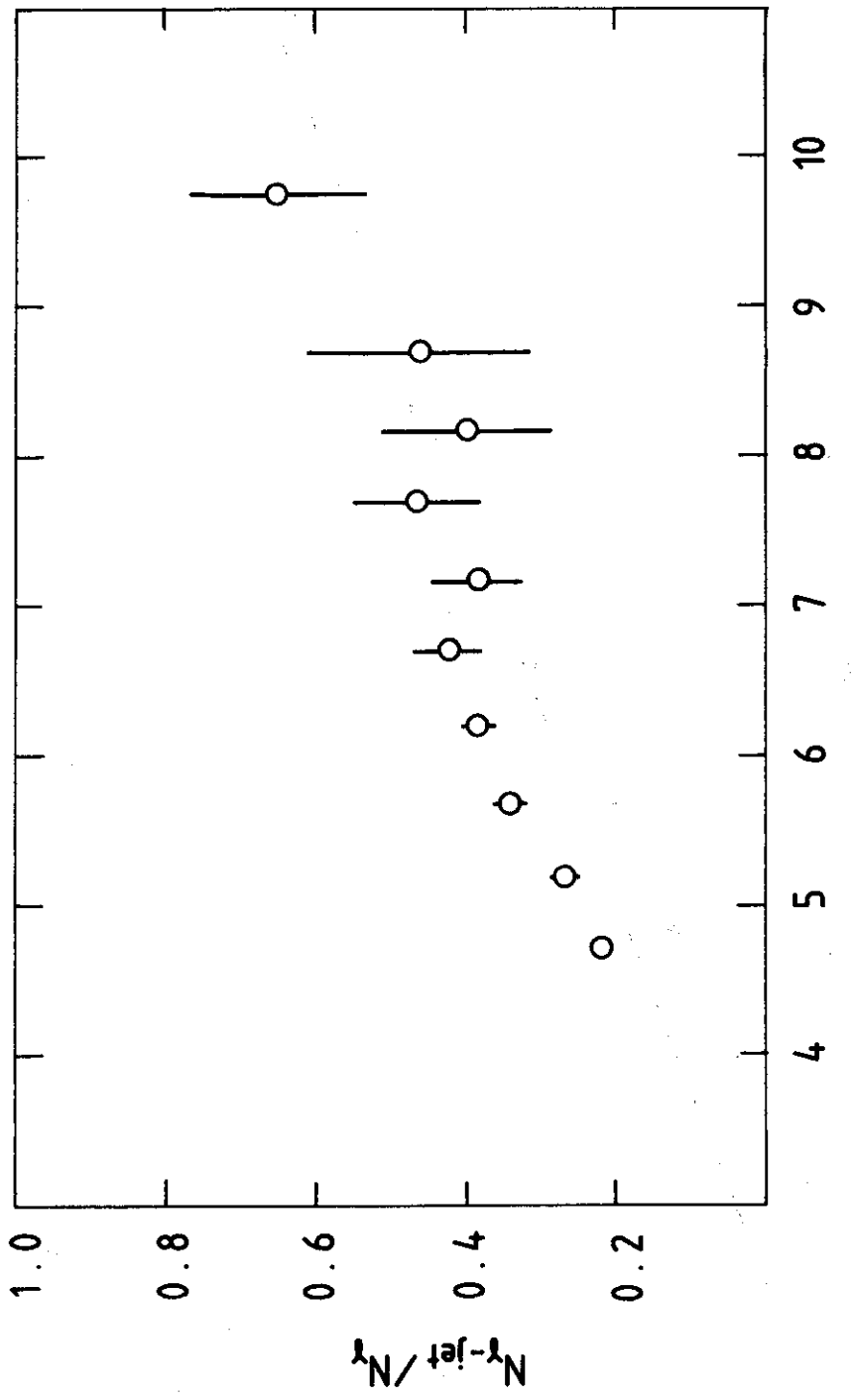


Fig. 8

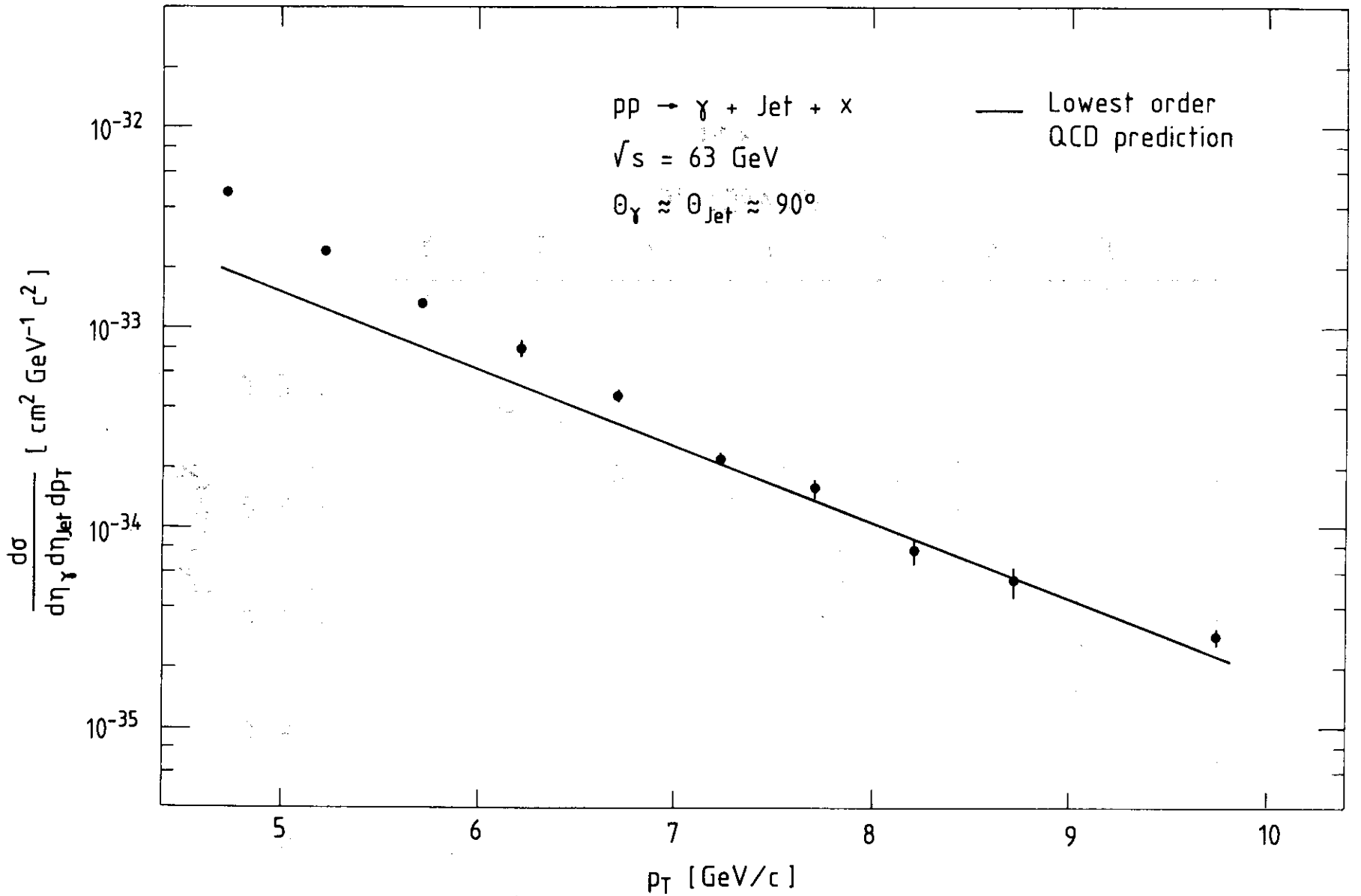
pp → γ + Jet + x
√s = 63 GeV
θγ ≈ θJet ≈ 90°
Lowest order
QCD prediction
10-32
10-33
10-34
10-35
5
6
7
8
9
10
pT [GeV/c]
dσ / dηγ dηJet dpT [cm2 GeV-1 c2]

**Fig. 9**

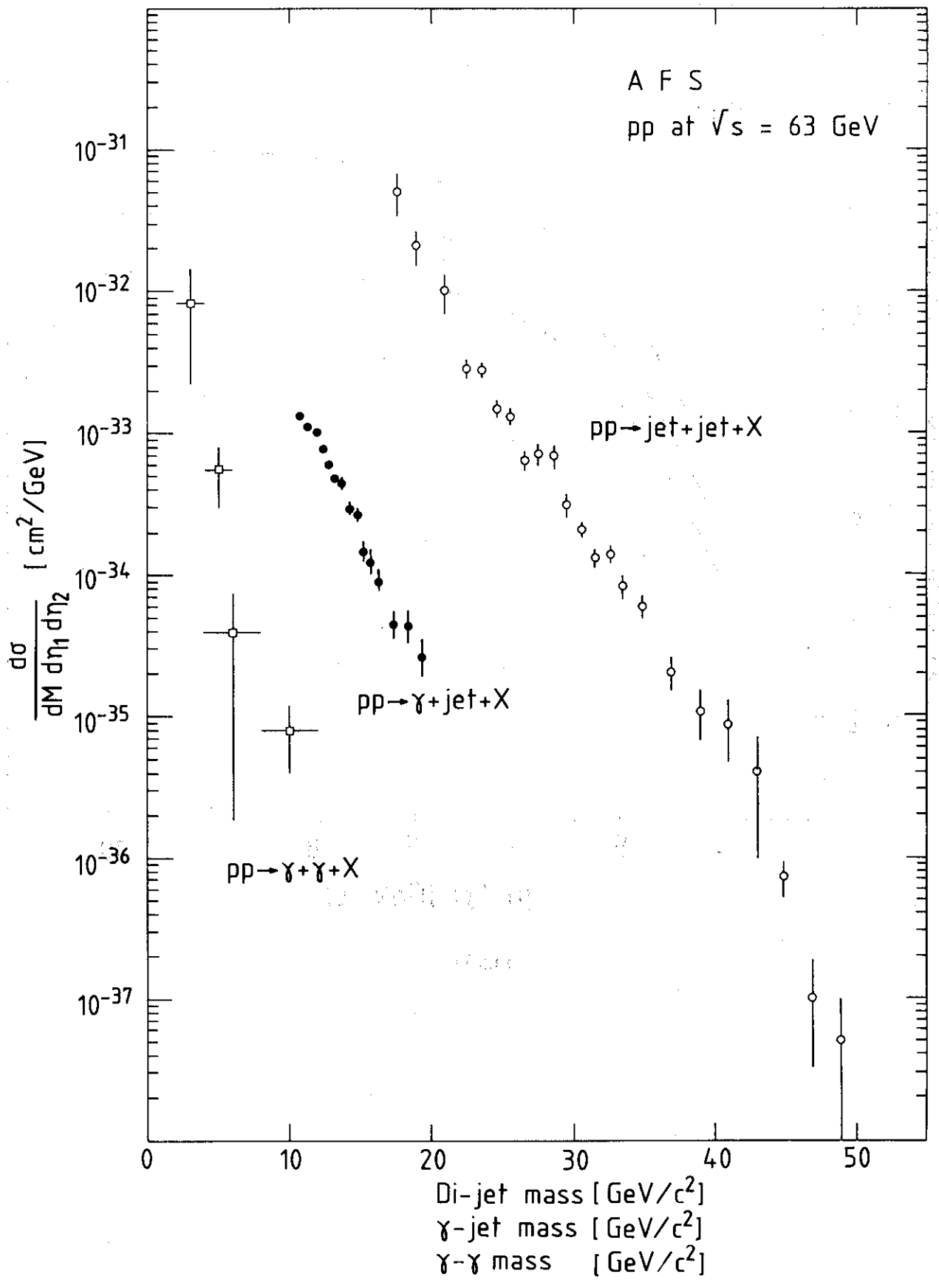
A F S
pp at √s = 63 GeV
pp→jet+jet+X
pp→γ+jet+X
pp→γ+γ+X
$\frac{d\sigma}{dM\,d\eta_1\,d\eta_2}$ [cm²/GeV]
Di-jet mass [GeV/c²]
γ-jet mass [GeV/c²]
γ-γ mass [GeV/c²]

**Fig. 10**

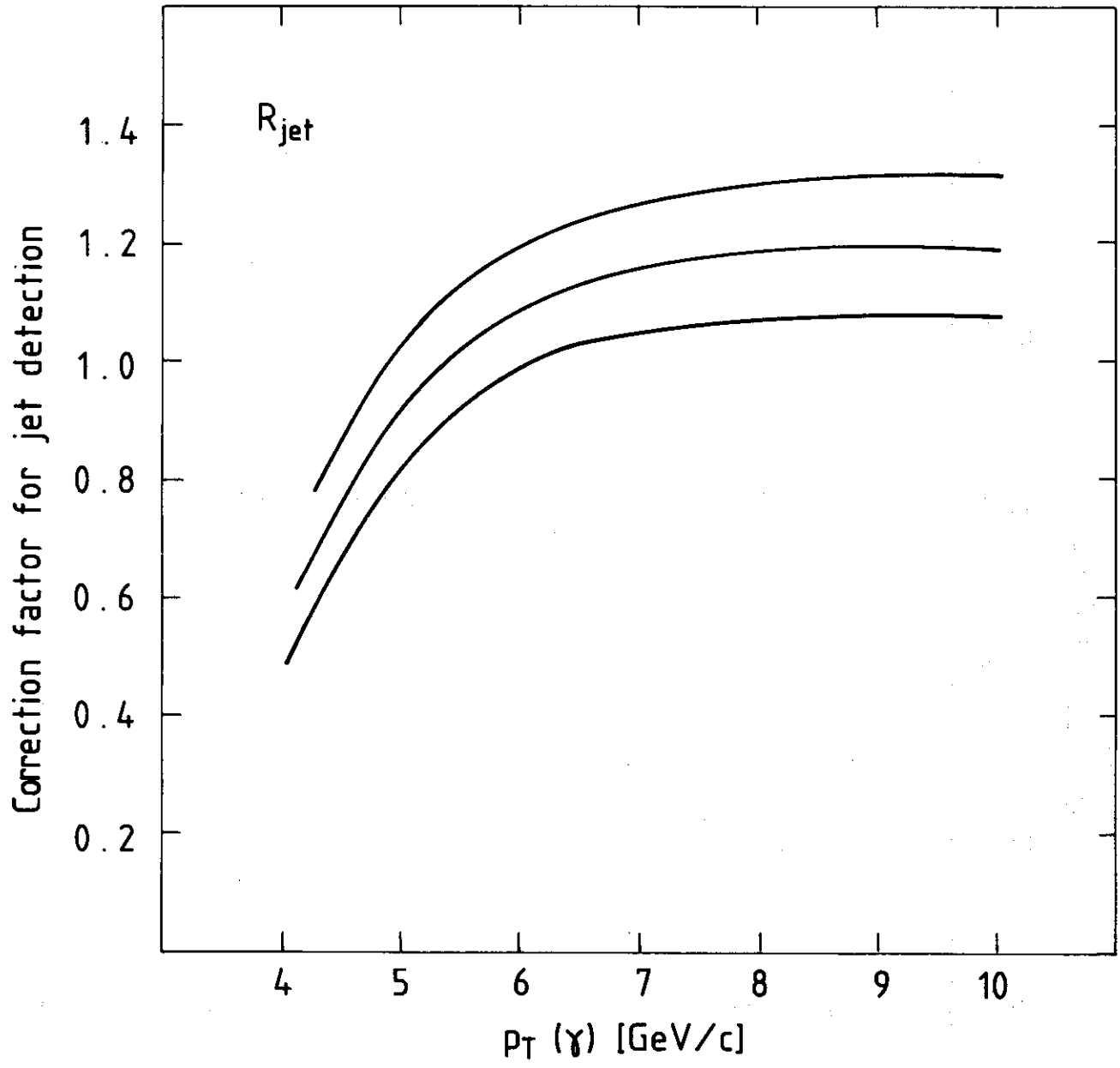
$R_{jet}$
Correction factor for jet detection
1.4
1.2
1.0
0.8
0.6
0.4
0.2
4
5
6
7
8
9
10
$p_T$ ($\gamma$) [GeV/c]

**Fig. 11**

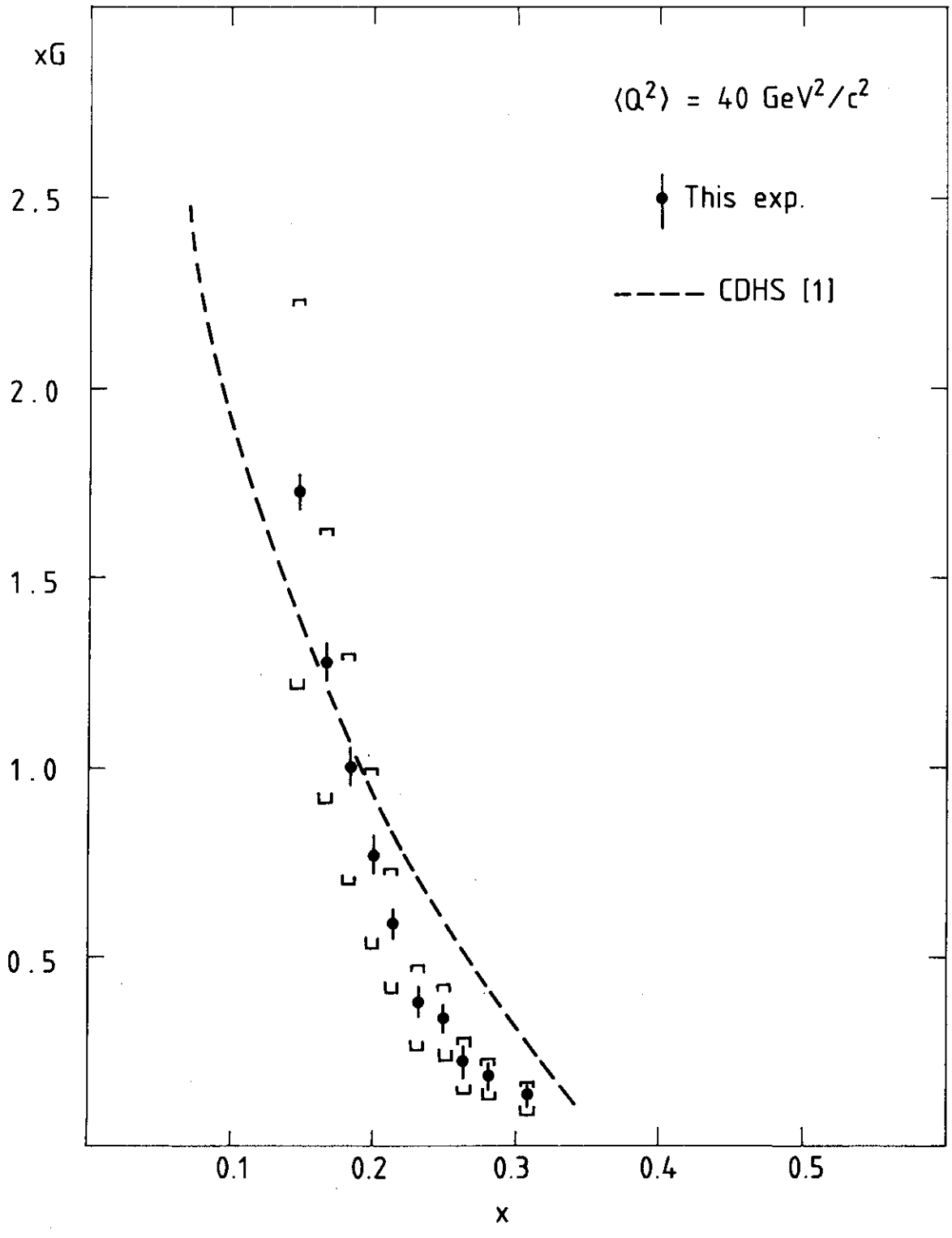
xG
$\langle Q^2 \rangle$ = 40 GeV$^2$/c$^2$
This exp.
CDHS [1]
2.5
2.0
1.5
1.0
0.5
0.1
0.2
0.3
0.4
0.5
x

**Fig. 12**